

---

# Compressive Sensing Based Synthesis of Multi-Beam Phased Array for Air Traffic Control

P. Rocca, N. Anselmi, M. A. Hannan and A. Massa

---

## Contents

<b>1 Numerical Assessment - Linear Array Synthesis</b>	<b>3</b>
1.1 $P = 2, \theta_1 = 90.75 \text{ deg}, \theta_2 = 96.57 \text{ deg}$ . . . . .	3
1.1.1 Solution: Best $M = 15$ . . . . .	5
1.1.2 MT-BCS errors . . . . .	8
1.2 $P = 3, \theta_1 = 84.93 \text{ deg}, \theta_2 = 90.75 \text{ deg}, \theta_3 = 96.57 \text{ deg}$ . . . . .	9
1.2.1 Solution: Best $M = 16$ . . . . .	11
1.2.2 MT-BCS errors . . . . .	15
1.3 $P = 4, \theta_1 = 79.06 \text{ deg}, \theta_2 = 84.93 \text{ deg}, \theta_3 = 90.75 \text{ deg}, \theta_4 = 96.57 \text{ deg}$ . . . . .	16
1.3.1 Solution: Best $M = 15$ . . . . .	18
1.3.2 MT-BCS errors . . . . .	23

# 1 Numerical Assessment - Linear Array Synthesis

## 1.1 $P = 2, \theta_1 = 90.75 \text{ deg}, \theta_2 = 96.57 \text{ deg}$

The test case has been performed using the parameter below.

Parameter	Values					
$\gamma_a$	0.100	0.309	0.954	2.947	9.103	
	10.985	33.932	104.811	323.746	1000.000	
$\gamma_b$	0.0001	0.00054	0.00295	0.01600	0.08685	
	0.47149	2.55955	13.89495	75.43120	100.00000	
Pattern Samples, $K$	22	24	26	28	30	32
	34	36	38	40	42	44
Aperture Samples, $N$	500	600	700	800	900	1000
Noise Variance, $\sigma$	0.000010	0.000031	0.000095	0.000295	0.000910	
	0.002812	0.008685	0.026827	0.082864	0.100000	

Table I: Simulation Parameters

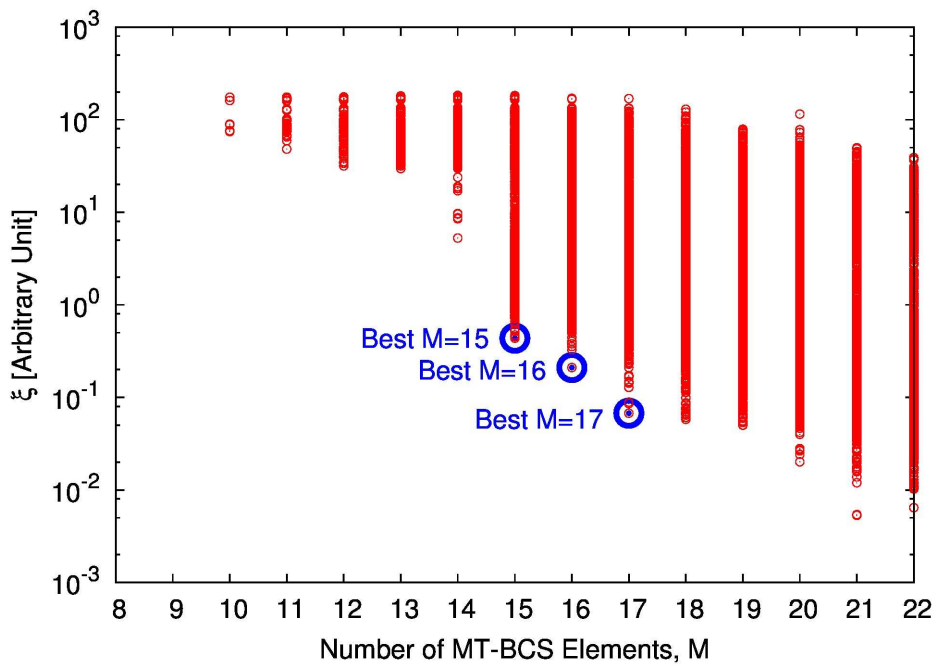


Figure 1: Output solutions from MT-BCS procedure

Fig.1 shows the solutions of the MT-BCS procedure having number of elements  $M \leq 22$ . The y-axis represents the mean error between the reference power patterns and the power pattern at the output of the MT-BCS.

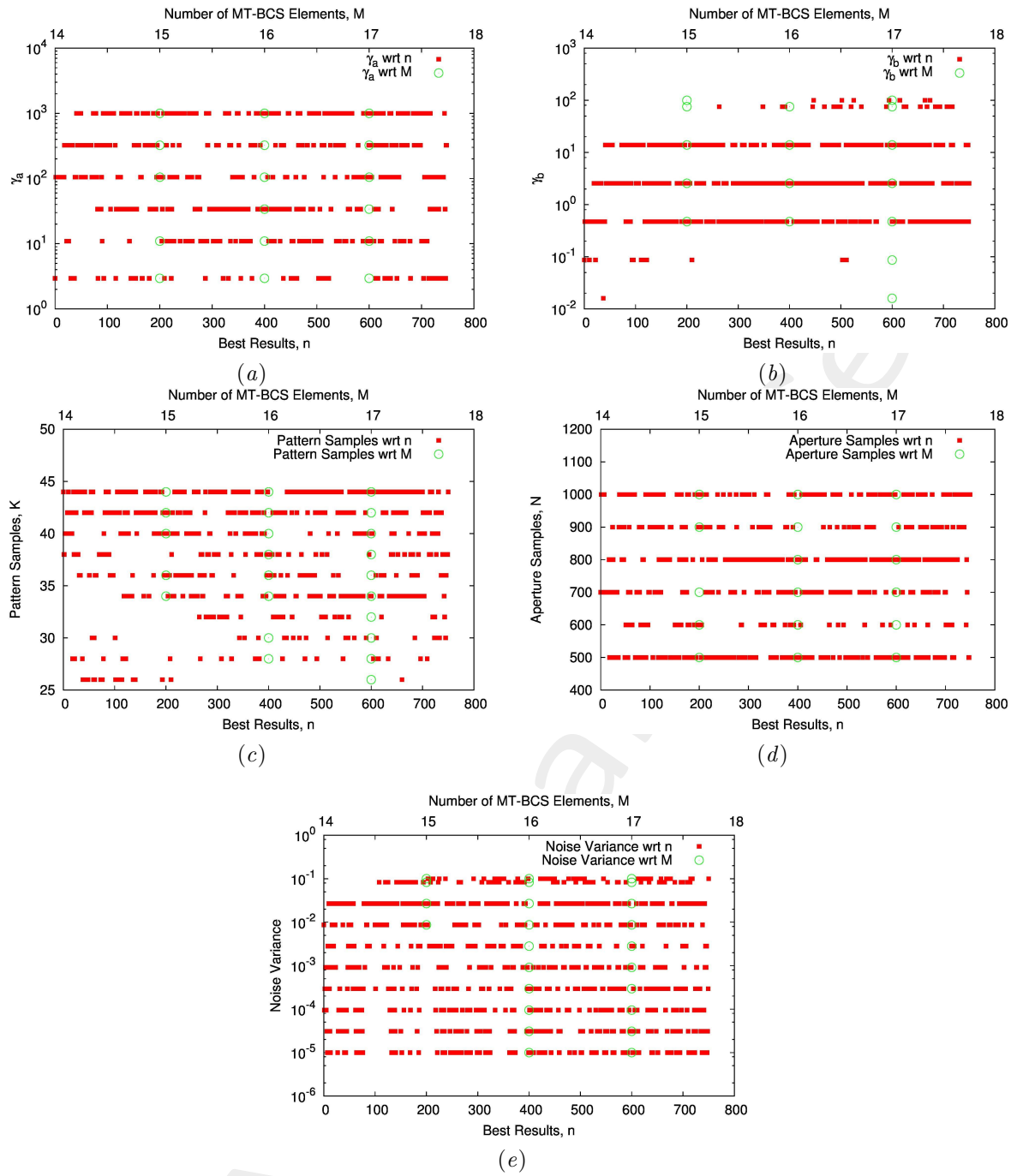


Figure 2: Parameters distribution, (a)  $\gamma_a$ , (b)  $\gamma_b$ , (c) Pattern Samples, (d) Aperture Samples, (e) Noise Variance

Fig. 2 shows parameter distributions as function of “Best results” (the ones with error value under  $8.0 \times 10^{-1}$  and number of MT-BCS elements lower than 19, sorted by error value) and number of elements.

---

### 1.1.1 Solution: Best $M = 15$

$\gamma_a$	$\gamma_b$	Pattern Samples [K]	Aperture Samples [N]	Noise Variance
323.746	13.89495	42	1000	0.026827

Table II: MT-BCS Input Parameters

In Tab. II are reported MT-BCS parameters of solution Best  $M = 15$ . Fig. 3 shows elements positions of MT-BCS sparse linear array obtained from solution  $M = 15$ .

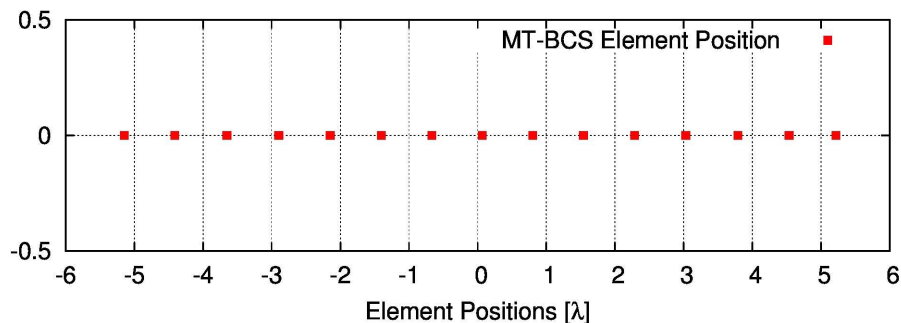


Figure 3: MT-BCS array elements positions

**Pattern**  $\theta_1 = 90.75 \text{ deg}$

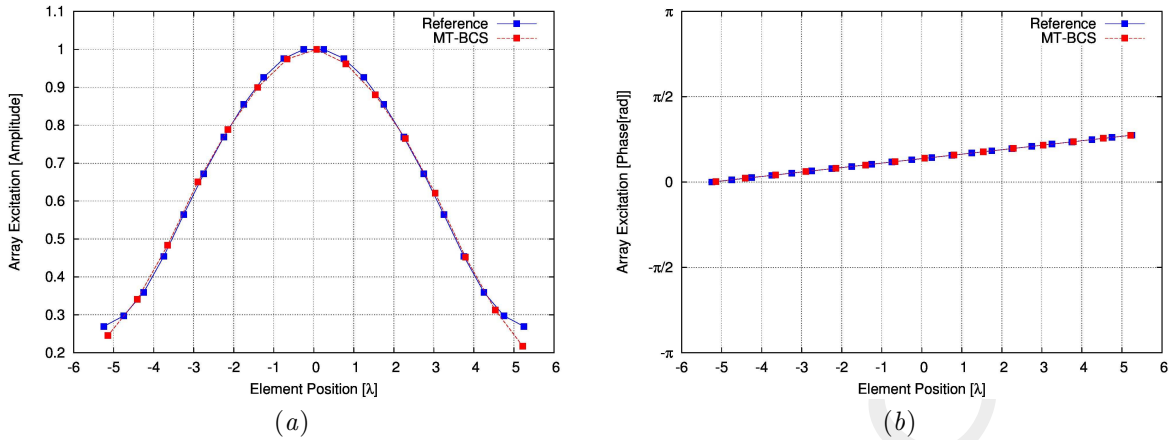


Figure 4: Array excitations, (a)Amplitudes, (b)Phases

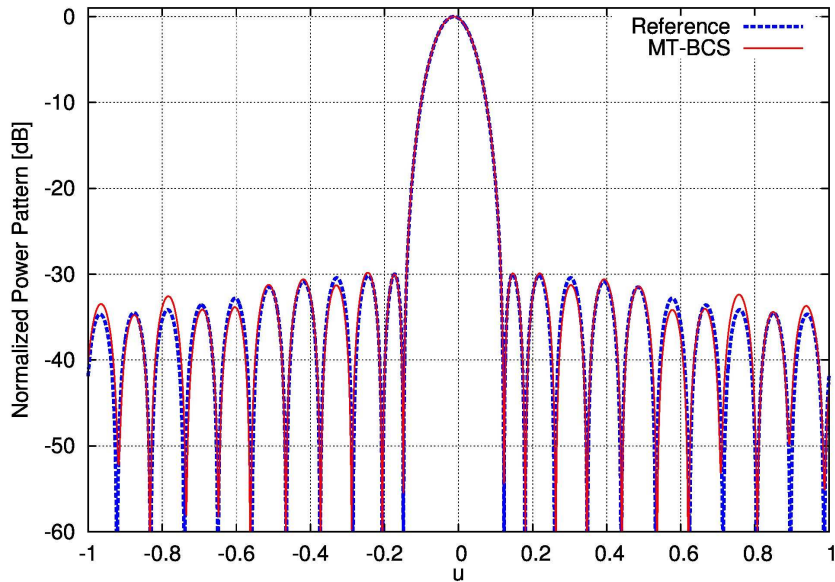


Figure 5: Power pattern comparison

Fig.4(a), 4(b) show comparison between Reference and MT-BCS amplitudes and phases excitations respectively.

Fig.5 shows the comparison between Reference and MT-BCS power pattern for the steereng angle  $\theta_1 = 90.75$  degrees.

	$SLL$ [dB]	$D$ [dB]	$HPBW$ [deg]	$M$	$err_1$
Reference	-29.99	12.76	5.82	22	—
MT - BCS	-29.81	12.75	5.84	15	$5.1194727 \times 10^{-1}$

Table III: Pattern  $\theta_1$ performance

In Tab.III comparison between Reference and MT-BCS power pattern performance parameters.

**Pattern**  $\theta_2 = 96.57 \text{ deg}$

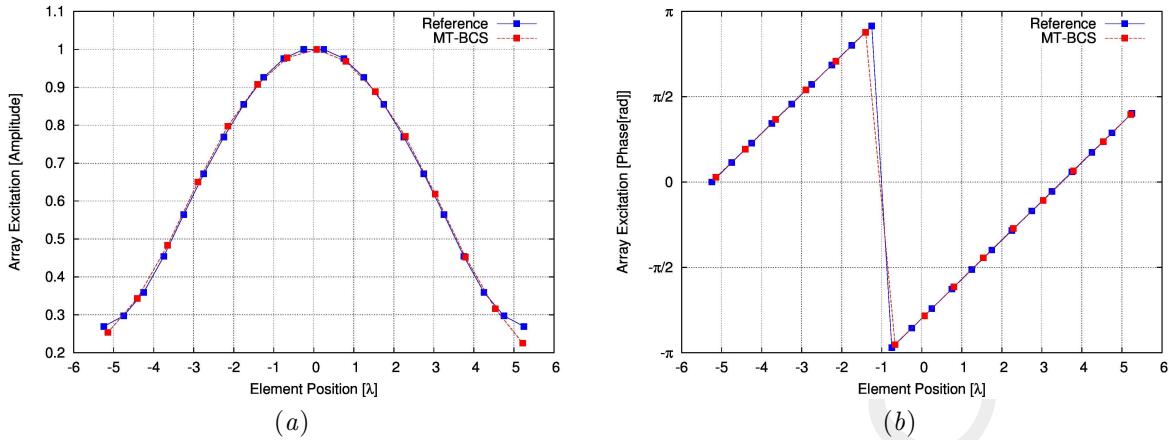


Figure 6: Array excitations, (a)Amplitudes, (b)Phases

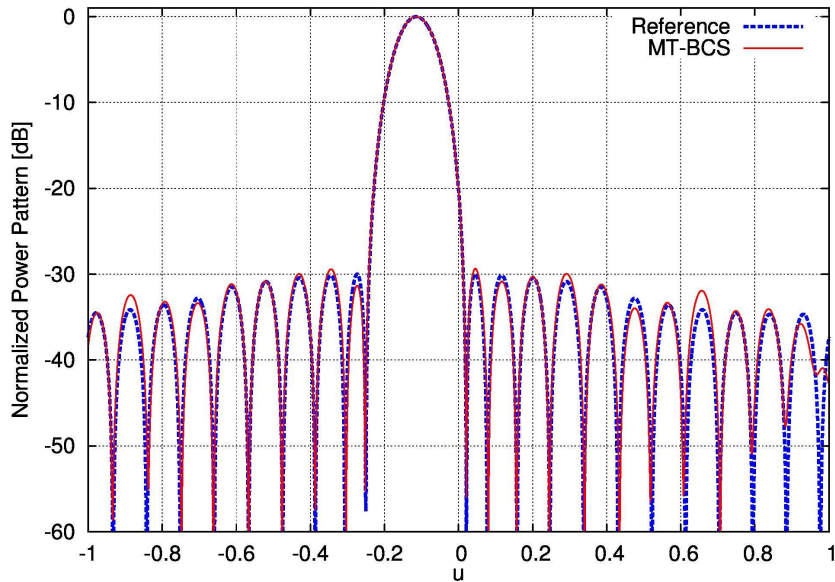


Figure 7: Power pattern comparison

Fig.6(a), 6(b) show comparison between Reference and MT-BCS amplitudes and phases excitations respectively.

Fig.7 shows the comparison between Reference and MT-BCS power pattern for the steereng angle  $\theta_2 = 96.57$  degrees.

	$SLL$ [dB]	$D$ [dB]	$HPBW$ [deg]	$M$	$err_2$
Reference	-29.99	12.76	5.86	22	—
MT – BCS	-29.35	12.75	5.87	15	$3.6014238 \times 10^{-1}$

Table IV: Pattern  $\theta_2$  performance

In Tab.IV comparison between Reference and MT-BCS power pattern performance parameters.

---

### 1.1.2 MT-BCS errors

In Tab.V are reported the error values. In particular:

- $I$ : total number of reference power pattern [ $I$ ];
- $\xi$ : total error of the entire procedure;
- $err_i$  ( $i = 1, \dots, I$ ): error on singular reference and MT-BCS pattern pair.

<i>Solution</i>	$err_1$	$err_2$
Best $M = 15$	$5.1194727 \times 10^{-1}$	$3.6014238 \times 10^{-1}$

<i>Solution</i>	$I$	$\xi$
Best $M = 15$	2	$4.360448 \times 10^{-1}$

Table V: MT-BCS errors

## 1.2 $P = 3$ , $\theta_1 = 84.93 \text{ deg}$ , $\theta_2 = 90.75 \text{ deg}$ , $\theta_3 = 96.57 \text{ deg}$

The test case has been performed using the parameters below.

Parameter	Values				
$\gamma_a$	0.100	0.309	0.954	2.947	9.103
	10.985	33.932	104.811	323.746	1000.000
$\gamma_b$	0.0001	0.000054	0.00295	0.01600	0.08685
	0.47149	2.55955	13.89495	75.43120	100.00000
Pattern Samples, $K$	22	24	26	28	30
	34	36	38	40	42
Aperture Samples, $N$	500	600	700	800	900
Noise Variance, $\sigma$	0.000010	0.000031	0.000095	0.000295	0.000910
	0.002812	0.008685	0.026827	0.082864	0.100000

Table VI: Simulation Parameters

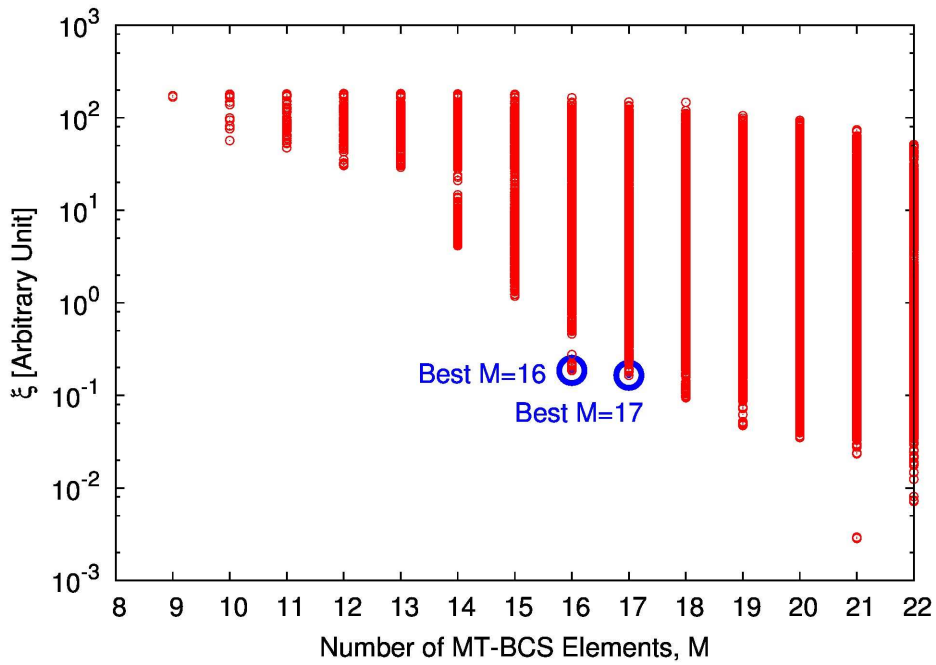


Figure 8: Output solutions from MT-BCS procedure

Fig.8 shows the solutions of the MT-BCS procedure having number of elements  $M \leq 22$ . The y-axis represents the mean error between the reference power patterns and the power pattern at the output of the MT-BCS.

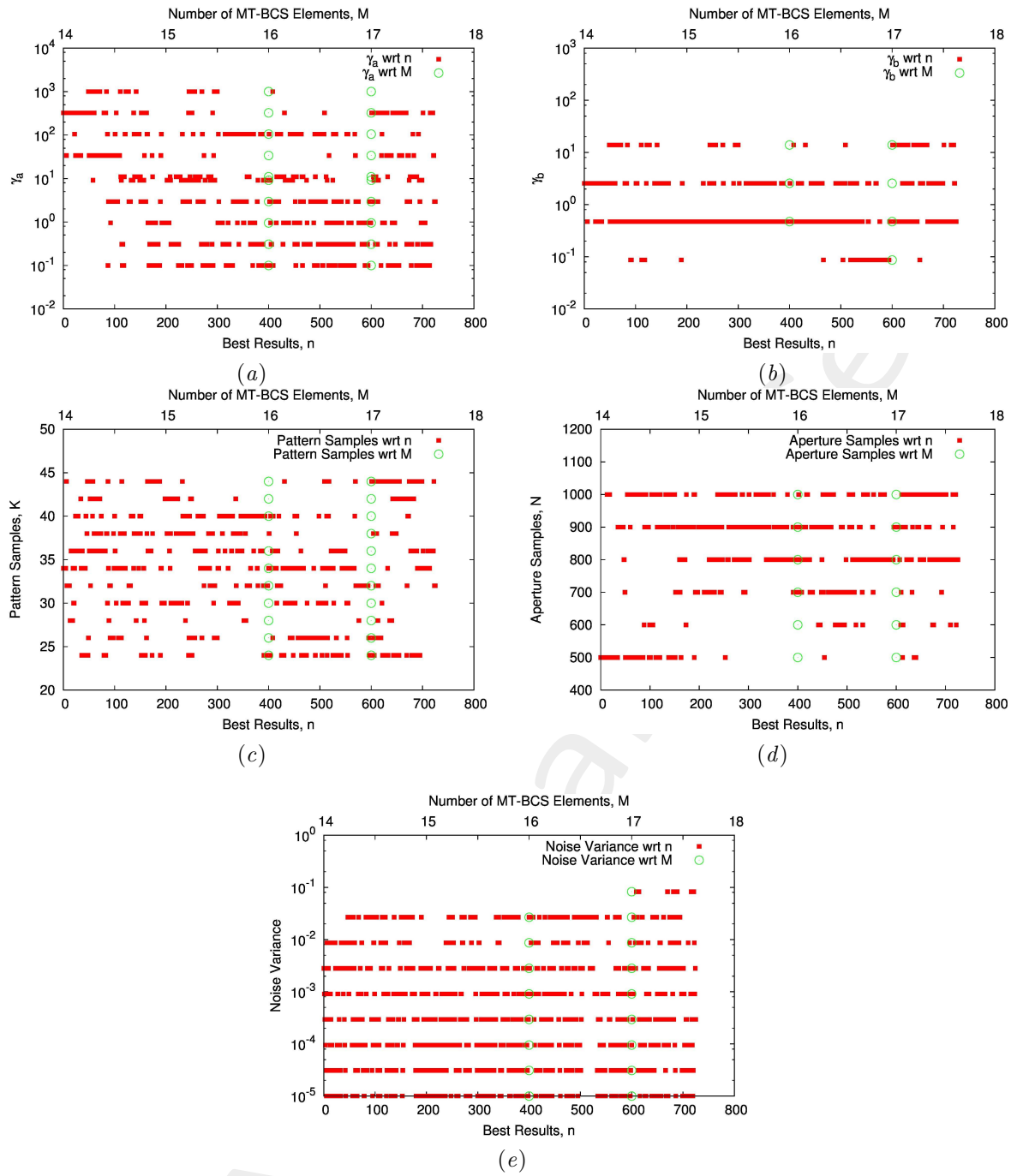


Figure 9: Parameters distribution, (a)  $\gamma_a$ , (b)  $\gamma_b$ , (c) Pattern Samples, (d) Aperture Samples, (e) Noise Variance

Fig. 9 shows parameter distributions as function of “Best Results” (the ones with error value under  $8.0 \times 10^{-1}$  and number of MT-BCS elements lower than 18, sorted by error value) and number of elements.

From Fig. 9 it is possible to notice that there are no “Best Results” with  $M = 15$  number of elements.

### 1.2.1 Solution: Best $M = 16$

$\gamma_a$	$\gamma_b$	Pattern Samples [K]	Aperture Samples [N]	Noise Variance
323.746	0.47149	44	500	0.008685

Table VII: MT-BCS Input Parameters

In Tab. VII are reported MT-BCS parameters of solution Best  $M = 16$ . Fig. 10 shows elements positions of MT-BCS sparse linear array obtained from solution Best  $M = 16$ .

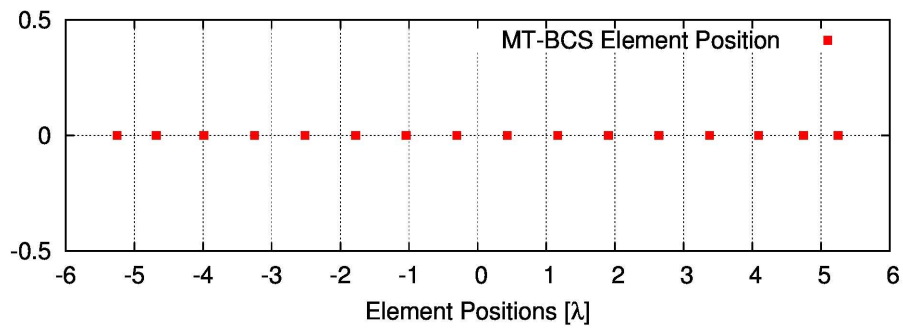


Figure 10: MT-BCS array elements positions

**Pattern**  $\theta_1 = 84.93 \text{ deg}$

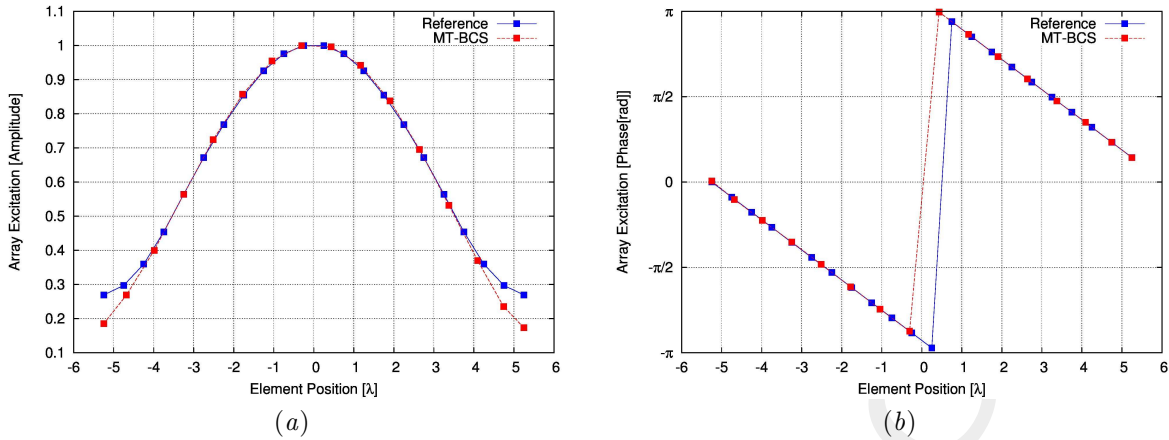


Figure 11: Array excitations, (a)Amplitudes, (b)Phases

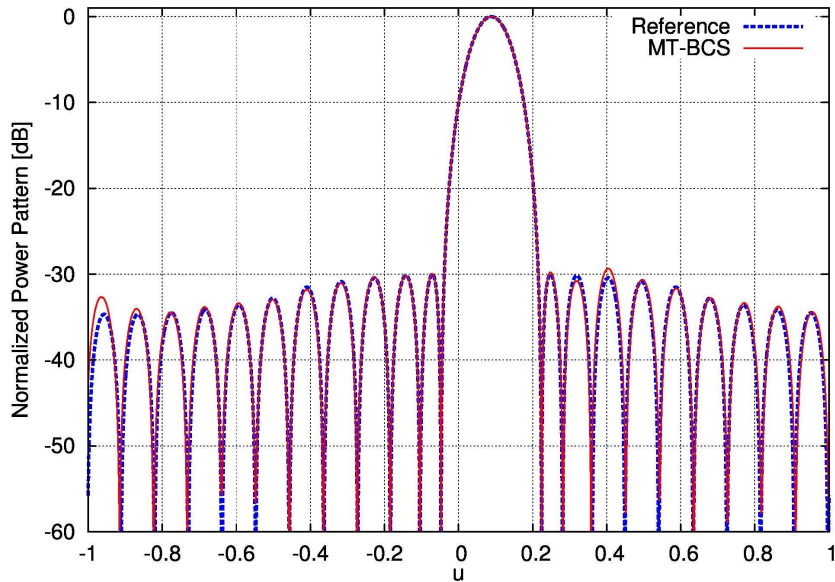


Figure 12: Power pattern comparison

Fig.11(a), 11(b) show comparison between Reference and MT-BCS amplitudes and phases excitations respectively.

Fig.12 shows the comparison between Reference and MT-BCS power pattern for the steereng angle  $\theta_1 = 84.93$  degrees.

	$SLL \text{ [dB]}$	$D \text{ [dB]}$	$HPBW \text{ [deg]}$	$M$	$err_1$
Reference	-29.99	12.77	5.84	22	—
MT - BCS	-29.34	12.76	5.85	16	$1.7800032 \times 10^{-1}$

Table VIII: Pattern  $\theta_1$  performance

In Tab.VIII comparison between Reference and MT-BCS power pattern performance parameters.

**Pattern  $\theta_2 = 90.75 \text{ deg}$**

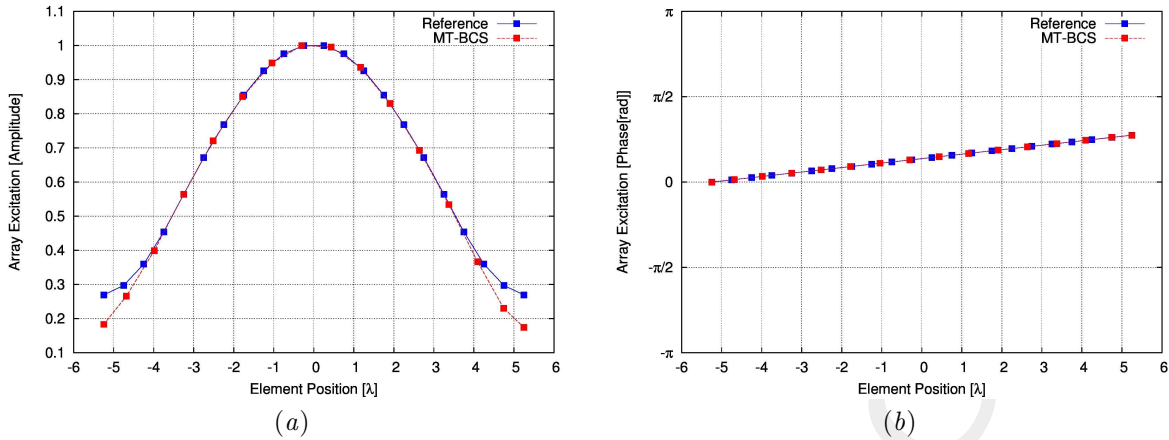


Figure 13: Array Excitations, (a)Amplitudes, (b)Phases

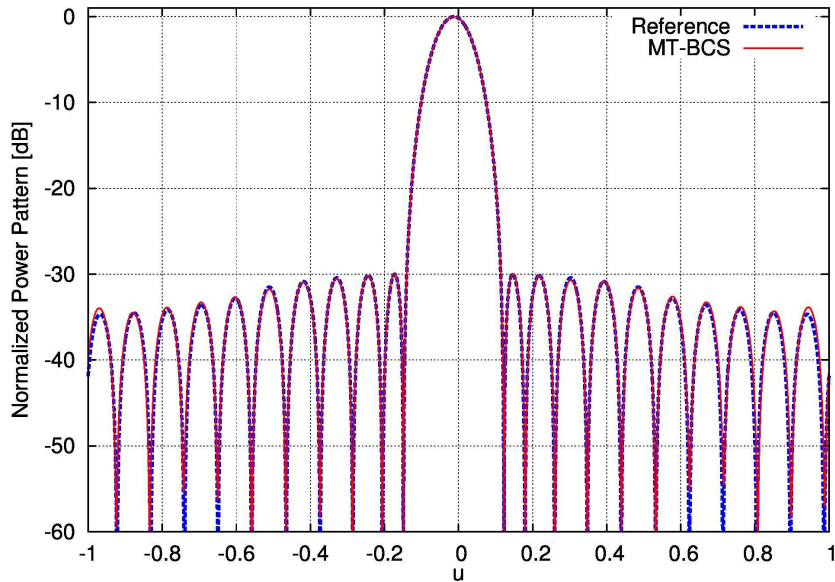


Figure 14: Power pattern comparison

Fig.13(a), 13(b) show comparison between Reference and MT-BCS amplitudes and phases excitations respectively.

Fig.14 shows the comparison between Reference and MT-BCS power pattern for the steereng angle  $\theta_2 = 90.75$  degrees.

	$SLL \text{ [dB]}$	$D \text{ [dB]}$	$HPBW \text{ [deg]}$	$M$	$err_2$
Reference	-29.99	12.77	5.82	22	—
MT – BCS	-29.92	12.76	5.83	16	$1.9301757 \times 10^{-1}$

Table IX: Pattern  $\theta_2$  performance

In Tab.IX comparison between Reference and MT-BCS power pattern performance parameters.

**Pattern**  $\theta_3 = 96.57 \text{ deg}$

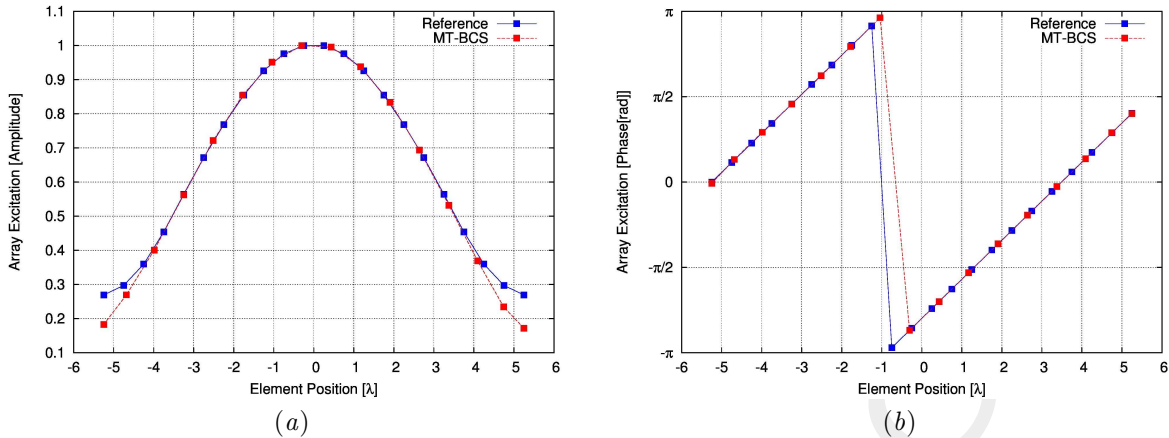


Figure 15: Array Excitations, (a)Amplitudes, (b)Phases

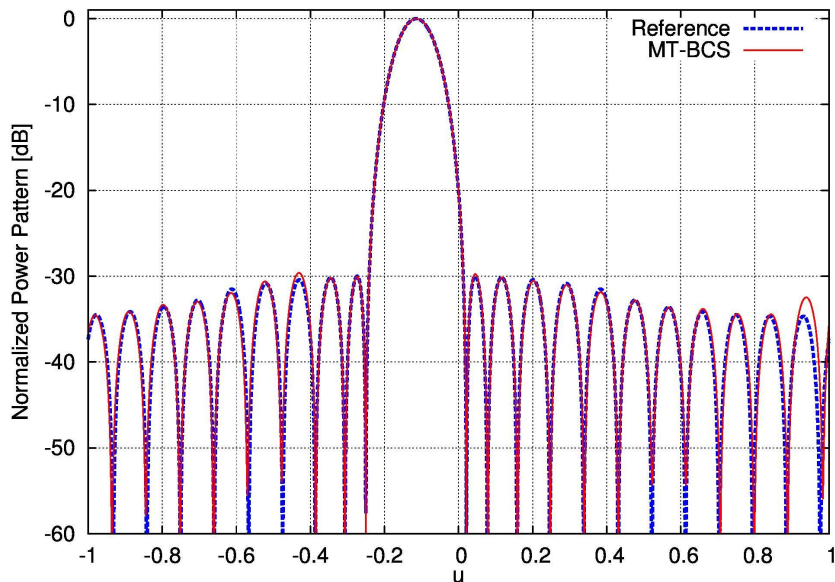


Figure 16: Power pattern comparison

Fig.15(a), 15(b) show comparison between Reference and MT-BCS amplitudes and phases excitations respectively.

Fig.16 shows the comparison between Reference and MT-BCS power pattern for the steereng angle  $\theta_3 = 96.57$  degrees.

	$SLL \text{ [dB]}$	$D \text{ [dB]}$	$HPBW \text{ [deg]}$	$M$	$err_3$
Reference	-29.99	12.77	5.86	22	—
MT – BCS	-29.61	12.76	5.87	16	$1.8657449 \times 10^{-1}$

Table X: Pattern  $\theta_3$  performance

In Tab.X comparison between Reference and MT-BCS power pattern performance parameters.

---

### 1.2.2 MT-BCS errors

In Tab.XI are reported the error values. In particular:

- $I$ : total number of reference power pattern [ $I$ ];
- $\xi$ : total error of the entire procedure;
- $err_i$  ( $i = 1, \dots, I$ ): error on singular reference and MT-BCS pattern pair.

<i>Solution</i>	$err_1$	$err_2$	$err_3$
Best $M = 16$	$1.7800032 \times 10^{-1}$	$1.9301757 \times 10^{-1}$	$1.8657449 \times 10^{-1}$

<i>Solution</i>	$I$	$\xi$
Best $M = 16$	3	$1.858641 \times 10^{-1}$

Table XI: MT-BCS errors

### 1.3 $P = 4$ , $\theta_1 = 79.06 \text{ deg}$ , $\theta_2 = 84.93 \text{ deg}$ , $\theta_3 = 90.75 \text{ deg}$ , $\theta_4 = 96.57 \text{ deg}$

The test case has been performed using the parameters below.

Parameter	Values				
$\gamma_a$	0.100	0.309	0.954	2.947	9.103
	10.985	33.932	104.811	323.746	1000.000
$\gamma_b$	0.0001	0.000054	0.00295	0.01600	0.08685
	0.47149	2.55955	13.89495	75.43120	100.00000
Pattern Samples, $K$	22	24	26	28	30
	34	36	38	40	42
Aperture Samples, $N$	500	600	700	800	900
Noise Variance, $\sigma$	0.000010	0.000031	0.000095	0.000295	0.000910
	0.002812	0.008685	0.026827	0.082864	0.100000

Table XII: Simulation Parameters

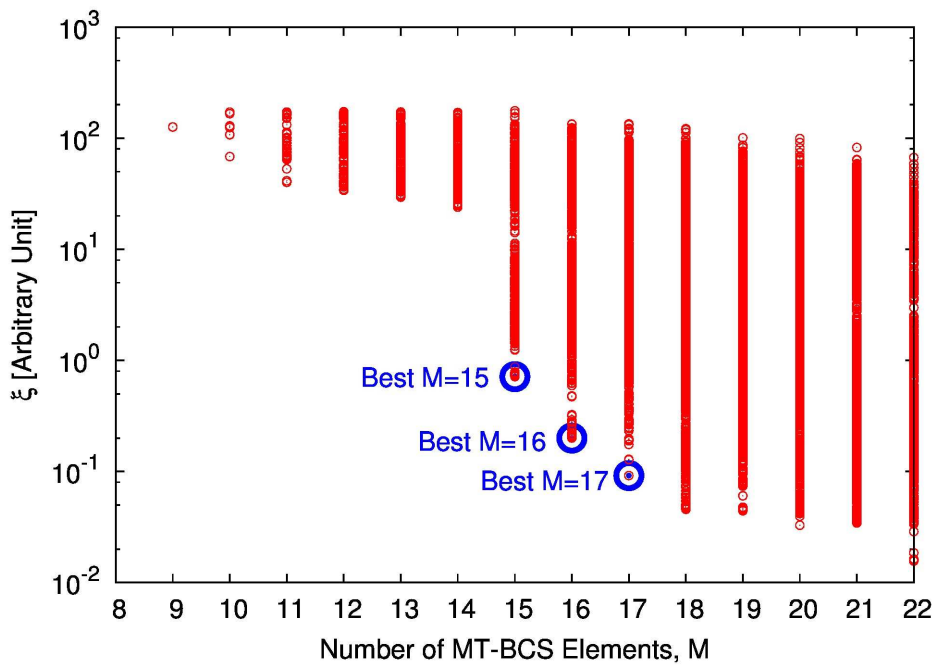


Figure 17: Output solutions from MT-BCS procedure

Fig.17 shows the solutions of the MT-BCS procedure having number of elements  $M \leq 22$ . The y-axis represents the mean error between the reference power patterns and the power pattern at the output of the MT-BCS.

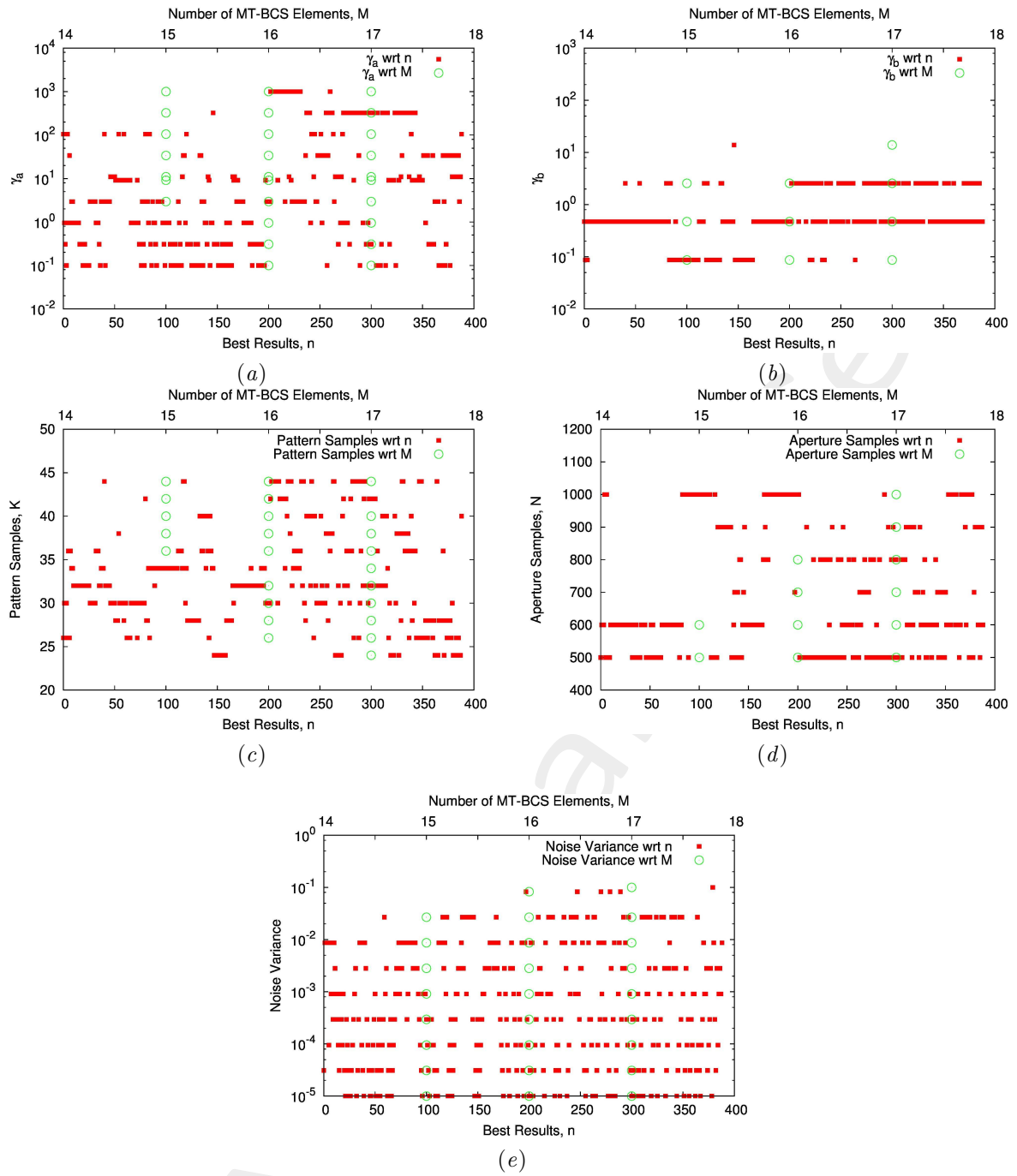


Figure 18: Parameters distribution, (a)  $\gamma_a$ , (b)  $\gamma_b$ , (c) Pattern Samples, (d) Aperture Samples, (e) Noise Variance

Fig.18 shows parameter distributions as function of “Best Results” (solutions with error value under  $8.0 \times 10^{-1}$  and number of MT-BCS elements lower than 18, sorted by error value) and number of elements.

### 1.3.1 Solution: Best $M = 15$

$\gamma_a$	$\gamma_b$	Pattern Samples [K]	Aperture Samples [N]	Noise Variance
104.811	0.47149	40	600	0.00091

Table XIII: MT-BCS Input Parameters

In Tab.XIII are reported MT-BCS parameters of solution Best  $M = 15$ . Fig.19 shows elements positions of MT-BCS sparse linear array obtained from solution Best  $M = 15$ .

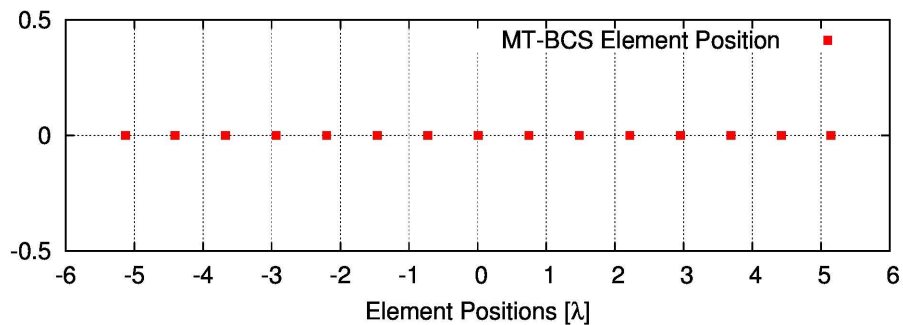


Figure 19: MT-BCS array elements positions

**Pattern**  $\theta_1 = 79.06 \text{ deg}$

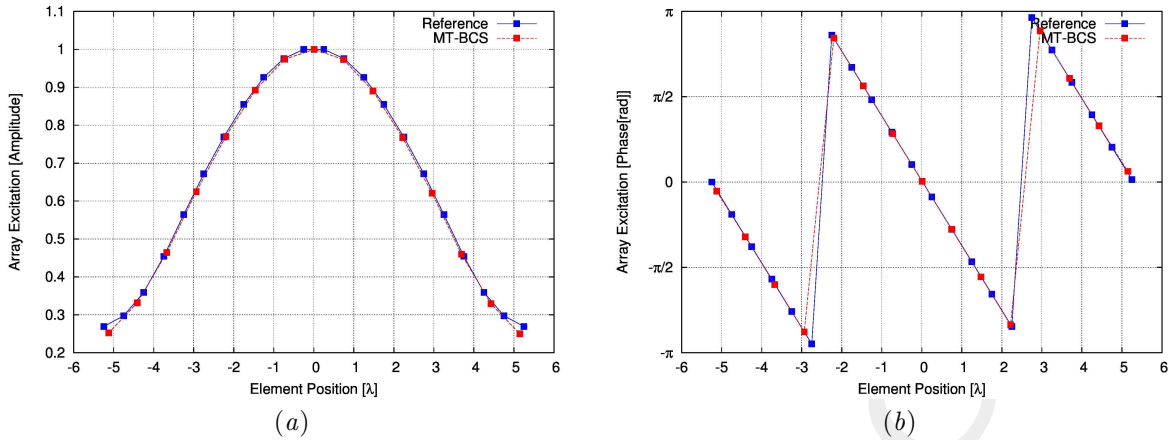


Figure 20: Array excitations, (a)Amplitudes, (b)Phases

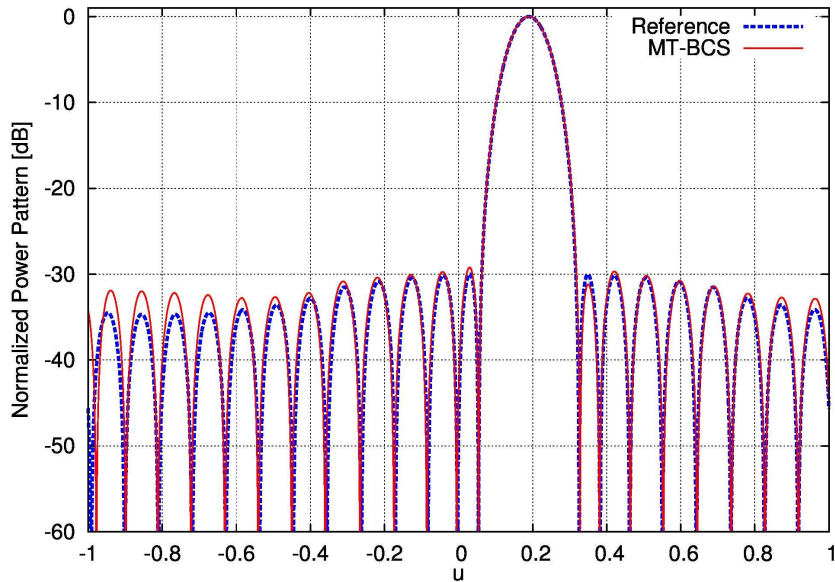


Figure 21: Power pattern comparison

Fig.20(a), 20(b) show comparison between Reference and MT-BCS amplitudes and phases excitations respectively.

Fig.21 shows the comparison between Reference and MT-BCS power pattern for the steereng angle  $\theta_1 = 79.06$  degrees.

	$SLL$ [dB]	$D$ [dB]	$HPBW$ [deg]	$M$	$err_1$
Reference	-29.99	12.76	5.93	22	—
MT – BCS	-29.22	12.74	5.97	15	$8.2470542 \times 10^{-1}$

Table XIV: Pattern  $\theta_1$  performance

In Tab.XIV comparison between Reference and MT-BCS power pattern performance parameters.

**Pattern**  $\theta_2 = 84.93 \text{ deg}$

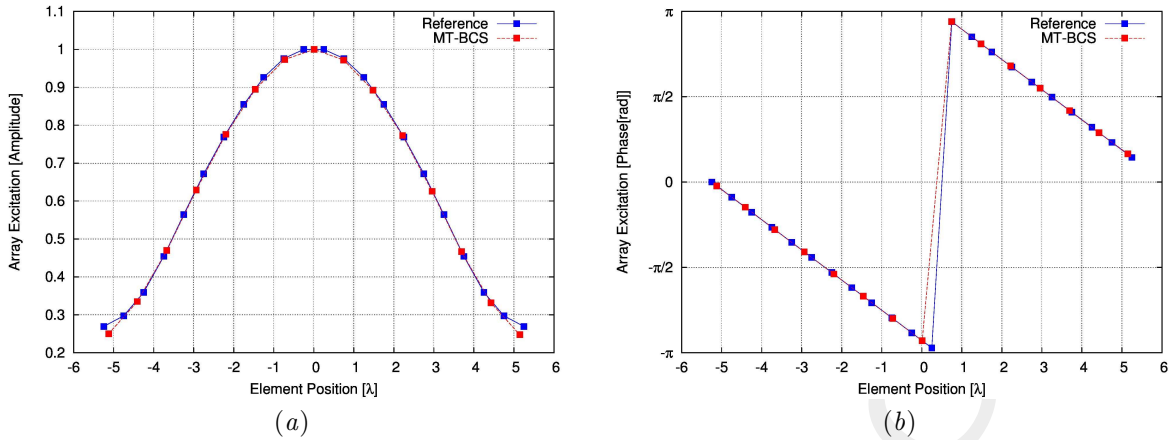


Figure 22: Array Excitations, (a)Amplitudes, (b)Phases

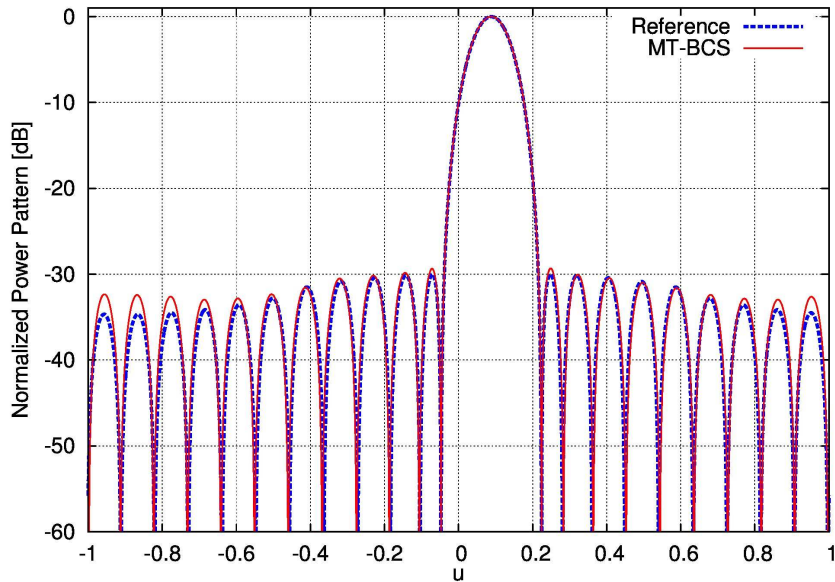


Figure 23: Power pattern comparison

Fig.22(a), 22(b) show comparison between Reference and MT-BCS amplitudes and phases excitations respectively.

Fig.23 shows the comparison between Reference and MT-BCS power pattern for the steereng angle  $\theta_2 = 84.93$  degrees.

	$SLL \text{ [dB]}$	$D \text{ [dB]}$	$HPBW \text{ [deg]}$	$M$	$err_2$
Reference	-29.99	12.77	5.84	22	—
MT - BCS	-29.31	12.74	5.88	15	$6.596669 \times 10^{-1}$

Table XV: Pattern  $\theta_2$ performance

In Tab.XV comparison between Reference and MT-BCS power pattern performance parameters.

**Pattern**  $\theta_3 = 90.75 \text{ deg}$

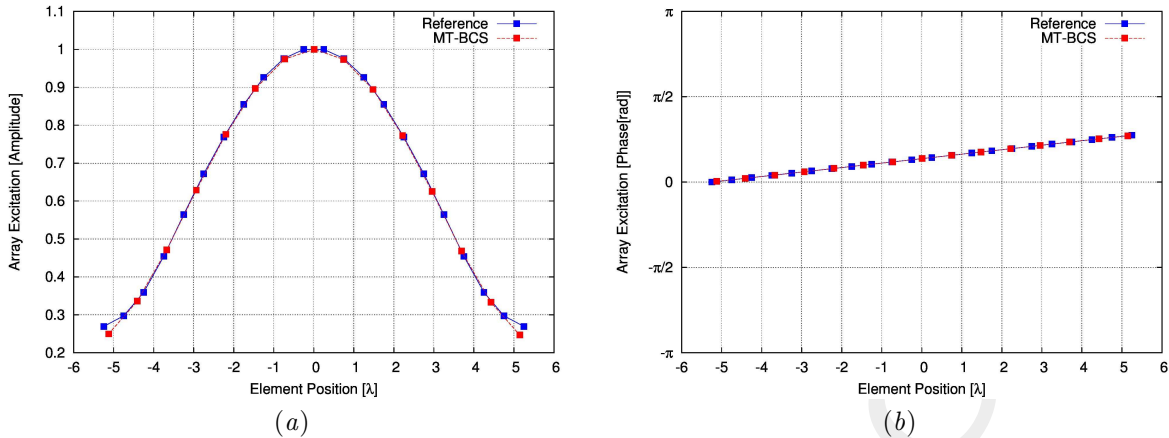


Figure 24: Array Excitations, (a)Amplitudes, (b)Phases

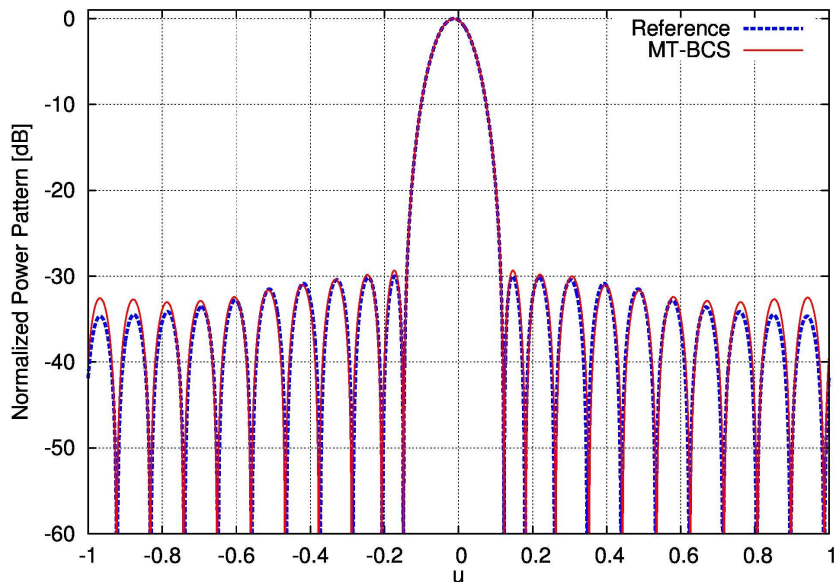


Figure 25: Power pattern comparison

Fig.24(a), 24(b) show comparison between Reference and MT-BCS amplitudes and phases excitations respectively.

Fig.25 shows the comparison between Reference and MT-BCS power pattern for the steereng angle  $\theta_3 = 90.75$  degrees.

	$SLL \text{ [dB]}$	$D \text{ [dB]}$	$HPBW \text{ [deg]}$	$M$	$err_3$
Reference	-29.99	12.77	5.82	22	—
MT – BCS	-29.36	12.74	5.85	15	$6.5778869 \times 10^{-1}$

Table XVI: Pattern  $\theta_3$  performance

In Tab.XVI comparison between Reference and MT-BCS power pattern performance parameters.

**Pattern**  $\theta_4 = 96.57 \text{ deg}$

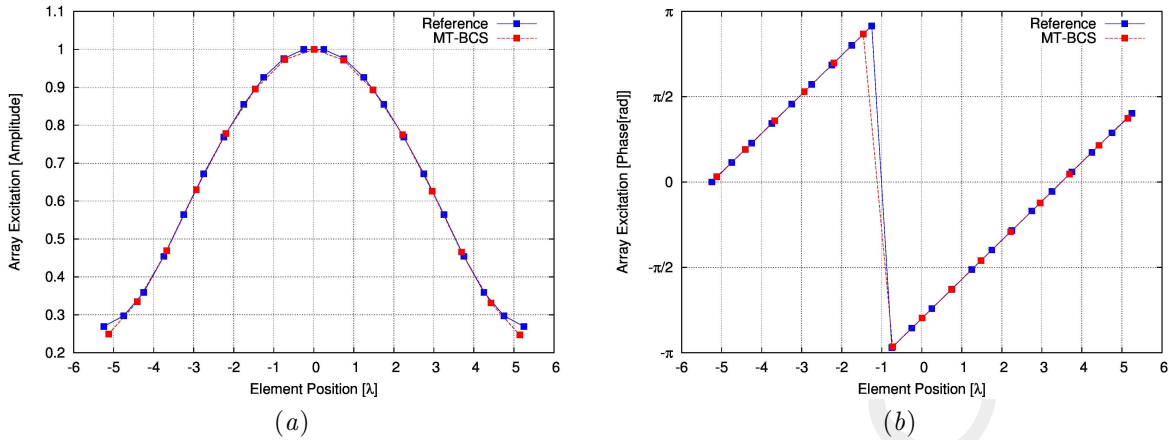


Figure 26: Array Excitations, (a)Amplitudes, (b)Phases

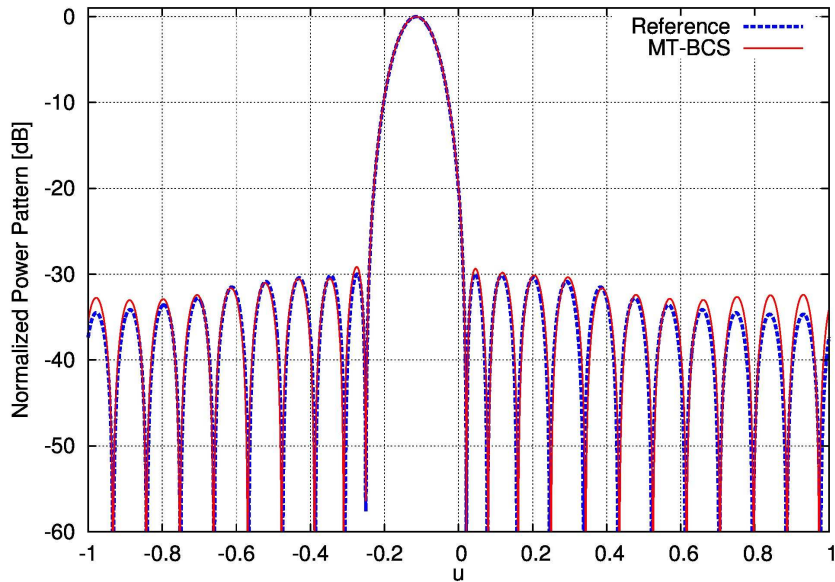


Figure 27: Power pattern comparison

Fig.26(a), 26(b) show comparison between Reference and MT-BCS amplitudes and phases excitations respectively.

Fig.27 shows the comparison between Reference and MT-BCS power pattern for the steereng angle  $\theta_4 = 96.57$  degrees.

	$SLL$ [dB]	$D$ [dB]	$HPBW$ [deg]	$M$	$err_4$
Reference	-29.99	12.77	5.86	22	—
MT – BCS	-29.16	12.74	5.89	15	$7.1513563 \times 10^{-1}$

Table XVII: Pattern  $\theta_4$  performance

In Tab.XVII comparison between Reference and MT-BCS power pattern performance parameters.

---

### 1.3.2 MT-BCS errors

In Tab.XVIII are reported the error values. In particular:

- $I$ : total number of reference power pattern [ $I$ ];
- $\xi$ : total error of the entire procedure;
- $err_i$  ( $i = 1, \dots, I$ ): error on singular reference and MT-BCS pattern pair.

<i>Solution</i>	$err_1$	$err_2$	$err_3$	$err_4$
Best $M = 15$	$8.247054 \times 10^{-1}$	$6.596669 \times 10^{-1}$	$6.577887 \times 10^{-1}$	$7.151356 \times 10^{-1}$

<i>Solution</i>	$I$	$\xi$
Best $M = 15$	4	$7.143242 \times 10^{-1}$

Table XVIII: MT-BCS errors

---

More information on the topics of this document can be found in the following list of references.

## References

- [1] P. Rocca, G. Oliveri, R. J. Mailloux, and A. Massa, "Unconventional phased array architectures and design Methodologies - A review," *Proceedings of the IEEE - Special Issue on 'Phased Array Technologies'*, Invited Paper, vol. 104, no. 3, pp. 544-560, March 2016.
- [2] A. Massa, P. Rocca, and G. Oliveri, "Compressive sensing in electromagnetics - A review," *IEEE Antennas Propag. Mag.*, pp. 224-238, vol. 57, no. 1, Feb. 2015.
- [3] F. Zardi, G. Oliveri, M. Salucci, and A. Massa, "Minimum-complexity failure correction in linear arrays via compressive processing," *IEEE Trans. Antennas Propag.*, vol. 69, no. 8, pp. 4504-4516, Aug. 2021.
- [4] N. Anselmi, G. Gottardi, G. Oliveri, and A. Massa, "A total-variation sparseness-promoting method for the synthesis of contiguously clustered linear architectures" *IEEE Trans. Antennas Propag.*, vol. 67, no. 7, pp. 4589-4601, Jul. 2019.
- [5] M. Salucci, A. Gelmini, G. Oliveri, and A. Massa, "Planar arrays diagnosis by means of an advanced Bayesian compressive processing," *IEEE Tran. Antennas Propag.*, vol. 66, no. 11, pp. 5892-5906, Nov. 2018.
- [6] L. Poli, G. Oliveri, P. Rocca, M. Salucci, and A. Massa, "Long-Distance WPT Unconventional Arrays Synthesis" *J. Electromagn. Waves Appl.*, vol. 31, no. 14, pp. 1399-1420, Jul. 2017.
- [7] G. Oliveri, M. Salucci, and A. Massa, "Synthesis of modular contiguously clustered linear arrays through a sparseness-regularized solver," *IEEE Trans. Antennas Propag.*, vol. 64, no. 10, pp. 4277-4287, Oct. 2016.
- [8] M. Carlin, G. Oliveri, and A. Massa, "Hybrid BCS-deterministic approach for sparse concentric ring isophoric arrays," *IEEE Trans. Antennas Propag.*, vol. 63, no. 1, pp. 378-383, Jan. 2015.
- [9] G. Oliveri, E. T. Bekele, F. Robol, and A. Massa, "Sparsening conformal arrays through a versatile BCS-based method," *IEEE Trans. Antennas Propag.*, vol. 62, no. 4, pp. 1681-1689, Apr. 2014.
- [10] F. Viani, G. Oliveri, and A. Massa, "Compressive sensing pattern matching techniques for synthesizing planar sparse arrays," *IEEE Trans. Antennas Propag.*, vol. 61, no. 9, pp. 4577-4587, Sept. 2013.
- [11] G. Oliveri, P. Rocca, and A. Massa, "Reliable diagnosis of large linear arrays - A Bayesian Compressive Sensing approach," *IEEE Trans. Antennas Propag.*, vol. 60, no. 10, pp. 4627-4636, Oct. 2012.
- [12] G. Oliveri, M. Carlin, and A. Massa, "Complex-weight sparse linear array synthesis by Bayesian Compressive Sampling," *IEEE Trans. Antennas Propag.*, vol. 60, no. 5, pp. 2309-2326, May 2012.
- [13] G. Oliveri and A. Massa, "Bayesian compressive sampling for pattern synthesis with maximally sparse non-uniform linear arrays," *IEEE Trans. Antennas Propag.*, vol. 59, no. 2, pp. 467-481, Feb. 2011.

- 
- [14] A. Benoni, P. Rocca, N. Anselmi, and A. Massa, "Hilbert-ordering based clustering of complex-excitations linear arrays," *IEEE Trans. Antennas Propag.*, vol. 70, no. 8, pp. 6751-6762, Aug. 2022.
  - [15] P. Rocca, L. Poli, N. Anselmi, and A. Massa, "Nested optimization for the synthesis of asymmetric shaped beam patterns in sub-arrayed linear antenna arrays," *IEEE Trans. Antennas Propag.*, vol. 70, no. 5, pp. 3385 - 3397, May 2022.
  - [16] P. Rocca, L. Poli, A. Polo, and A. Massa, "Optimal excitation matching strategy for sub-arrayed phased linear arrays generating arbitrary shaped beams," *IEEE Trans. Antennas Propag.*, vol. 68, no. 6, pp. 4638-4647, Jun. 2020.
  - [17] G. Oliveri, G. Gottardi and A. Massa, "A new meta-paradigm for the synthesis of antenna arrays for future wireless communications," *IEEE Trans. Antennas Propag.*, vol. 67, no. 6, pp. 3774-3788, Jun. 2019.
  - [18] P. Rocca, M. H. Hannan, L. Poli, N. Anselmi, and A. Massa, "Optimal phase-matching strategy for beam scanning of sub-arrayed phased arrays," *IEEE Trans. Antennas Propag.*, vol. 67, no. 2, pp. 951-959, Feb. 2019.
  - [19] N. Anselmi, P. Rocca, M. Salucci, and A. Massa, "Contiguous phase-clustering in multibeam-on-receive scanning arrays" *IEEE Trans. Antennas Propag.*, vol. 66, no. 11, pp. 5879-5891, Nov. 2018.
  - [20] L. Poli, G. Oliveri, P. Rocca, M. Salucci, and A. Massa, "Long-distance WPT unconventional arrays synthesis" *J. Electromagn. Waves Appl.*, vol. 31, no. 14, pp. 1399-1420, Jul. 2017.
  - [21] G. Gottardi, L. Poli, P. Rocca, A. Montanari, A. Aprile, and A. Massa, "Optimal monopulse beamforming for side-looking airborne radars," *IEEE Antennas Wirel. Propag. Lett.*, vol. 16, pp. 1221-1224, 2017.
  - [22] P. Rocca, M. D'Urso, and L. Poli, "Advanced strategy for large antenna array design with subarray-only amplitude and phase contr," *IEEE Antennas and Wirel. Propag. Lett.*, vol. 13, pp. 91-94, 2014.
  - [23] L. Manica, P. Rocca, G. Oliveri, and A. Massa, "Synthesis of multi-beam sub-arrayed antennas through an excitation matching strategy," *IEEE Trans. Antennas Propag.*, vol. 59, no. 2, pp. 482-492, Feb. 2011.
  - [24] M. Salucci, G. Oliveri, and A. Massa, "An innovative inverse source approach for the feasibility-driven design of reflectarrays," *IEEE Trans. Antennas Propag.*, vol. 70, no. 7, pp. 5468-5480, July 2022.
  - [25] L. T. P. Bui, N. Anselmi, T. Isernia, P. Rocca, and A. F. Morabito, "On bandwidth maximization of fixed-geometry arrays through convex programming," *J. Electromagn. Waves Appl.*, vol. 34, no. 5, pp. 581-600, 2020.
  - [26] N. Anselmi, L. Poli, P. Rocca, and A. Massa, "Design of simplified array layouts for preliminary experimental testing and validation of large AESAs," *IEEE Trans. Antennas Propag.*, vol. 66, no. 12, pp. 6906-6920, Dec. 2018.
  - [27] G. Oliveri and T. Moriyama, "Hybrid PS-CP technique for the synthesis of n-uniform linear arrays with maximum directivity" *J. Electromagn. Waves Appl.*, vol. 29, no. 1, pp. 113-123, Jan. 2015.

- 
- [28] P. Rocca and A. Morabito, "Optimal synthesis of reconfigurable planar arrays with simplified architectures for monopulse radar applications" *IEEE Trans. Antennas Propag.*, vol. 63, no. 3, pp. 1048-1058, Mar. 2015.
  - [29] A. F. Morabito and P. Rocca, "Reducing the number of elements in phase-only reconfigurable arrays generating sum and difference patterns," *IEEE Antennas Wireless Propag. Lett.*, vol. 14, pp. 1338-1341, 2015.
  - [30] P. Rocca, N. Anselmi, and A. Massa, "Optimal synthesis of robust beamformer weights exploiting interval analysis and convex optimization," *IEEE Trans. Antennas Propag.*, vol. 62, no. 7, pp. 3603-3612, Jul. 2014.
  - [31] G. Oliveri, G. Gottardi, M. A. Hannan, N. Anselmi, and L. Poli, "Autocorrelation-driven synthesis of antenna arrays - The case of DS-based planar isophoric thinned arrays," *IEEE Trans. Antennas Propag.*, vol. 68, no. 4, pp. 2895-2910, Apr. 2020.
  - [32] M. Salucci, G. Gottardi, N. Anselmi, and G. Oliveri, "Planar thinned array design by hybrid analytical-stochastic optimization," *IET Microw. Antennas Propag.*, vol. 11, no. 13, pp. 1841-1845, Oct. 2017
  - [33] T. Moriyama, E. Giarola, M. Salucci, and G. Oliveri, "On the radiation properties of ADS-thinned dipole arrays" *IEICE Electronics Express*, vol. 11, no. 16, pp. 1-10, Aug. 2014.
  - [34] G. Oliveri, F. Viani, and A. Massa, "Synthesis of linear multi-beam arrays through hierarchical ADS-based interleaving," *IET Microw. Antennas Propag.*, vol. 8, no. 10, pp. 794-808, Jul. 2014.
  - [35] D. Sartori, G. Oliveri, L. Manica, and A. Massa, "Hybrid Design of non-regular linear arrays with accurate control of the pattern sidelobes," *IEEE Trans. Antennas Propag.*, vol. 61, no. 12, pp. 6237-6242, Dec. 2013.